

Opto-Mechanical Design of the Gemini Multi-Object Spectrograph On-Instrument Wavefront Sensor

Scott Roberts^a, Murray Fletcher, Brian Leckie, Les Saddlemyer, Kei Szeto, Jerry Sebesta

Dominion Astrophysical Observatory, Herzberg Institute of Astrophysics,
National Research Council Canada

ABSTRACT

The Gemini^b Multi-Object Spectrographs (GMOS)¹ will exploit the excellent delivered image quality of the Gemini 8-metre telescopes. An integral part of the GMOS optical design is the On-Instrument Wavefront Sensor (OIWFS). The OIWFS measures image tip-tilt and focus (TTF) information and feeds this back to the telescope's active and adaptive optics systems. Since GMOS is Cassegrain mounted, the OIWFS was designed to be insensitive to the varying gravity vector as the telescope tracks. The OIWFS utilizes a two-rotational-axis robotic platform to position the pickoff optics within the telescope field. The mechanical design, optics, kinematics and an analysis of the optical measurement error due to mechanical flexure of the OIWFS are presented.

Keywords: wavefront sensor, spectrograph, optics, kinematics, flexure

1. INTRODUCTION

The Gemini 8-metre optical telescopes, located on Mauna Kea, Hawaii, and Cerro Pachon, Chile, are designed to exploit the excellent atmospheric seeing at these sites. Each telescope will be equipped with a multi-object spectrograph (GMOS). The GMOS instrument is designed for imaging as well as multi-slit and integral field spectroscopy of a 5.5 arcminute square field in the wavelength range of 0.37 to 1.1 microns. An integral part of the GMOS instrument is the On-Instrument Wavefront Sensor (OIWFS). The OIWFS analyses the image of a guide star at the slit plane to measure and feed-back tip, tilt and focus information to the telescope control system. Feedback from the OIWFS minimizes focus errors at the slit plane and keeps objects centred on the spectrograph slits. Since the scientific specifications require that GMOS deliver radial velocities of 2 km/s in multi-slit mode, the error budget for the OIWFS is very tight. The OIWFS system, mechanics, optics, and electronics, must contribute less than $2.05 \mu\text{m/hr}$ of guide star positional error at the telescope focal plane, hereafter referred to as the slit plane.

Figure 1 shows the OIWFS integrated with the GMOS slit plane environment. The OIWFS can be seen on the left with the pickoff arm and optic deployed at the slit plane. Slit masks and Integral Field Units², fibre-optic systems that can be deployed at the slit plane to provide two-dimensional spectroscopy over a small field, are stored on the cassette stage and can be automatically selected and deployed onto the slit plane.

Figure 2 shows the On-Instrument Wavefront Sensor. The wavefront sensor (WFS) utilizes a two-axis rotational stage to position a pickoff arm, mirror and wavefront sensor in the GMOS field. The WFS consists of a lenslet array coupled to a thermoelectrically-cooled charge coupled device (CCD). Wiring and glycol lines, for removing heat from the WFS, pass from the stationary CCD controller through an umbilical cable to the wavefront sensor. The OIWFS patrols the GMOS field in a plane 75 mm offset towards the Instrument Support Structure (ISS) from the telescope focus. This offset provides clearance for Integral Field Units at the slit plane.

^a Further author information - S.R. (correspondence). Email: scott.roberts@hia.nrc.ca; Address: 5071 West Saanich Road, Victoria, B.C., Canada, V8X-4M6; Telephone: 250-363-0051; Fax: 250-363-0045

^b The Gemini 8-m Telescopes Project is managed by the Association of Universities for Research in Astronomy, for the National Science Foundation, under an international partnership agreement.

The pickoff arm positions a small internally reflecting prism in front of the GMOS slit plane to redirect the guide-star light to the wavefront sensor. The arm is designed to be as stiff as possible with the constraint that the vignetting must be at most 5% of the focal plane area. This led to the design choice of a cantilevered, tapered beam.

In order to meet the stringent mechanical flexure requirements, a positioning system incorporating two rotational stages was chosen. In this design, the rotational stages are mass-balanced in torque and moment to minimize deflections due to a varying gravity vector. The design of the stage and pickoff system minimizes the measurement error at the WFS and not necessarily the absolute flexure of the OIWFS structure. There is a distinction because the wavefront sensor has varying sensitivity to flexure modes.

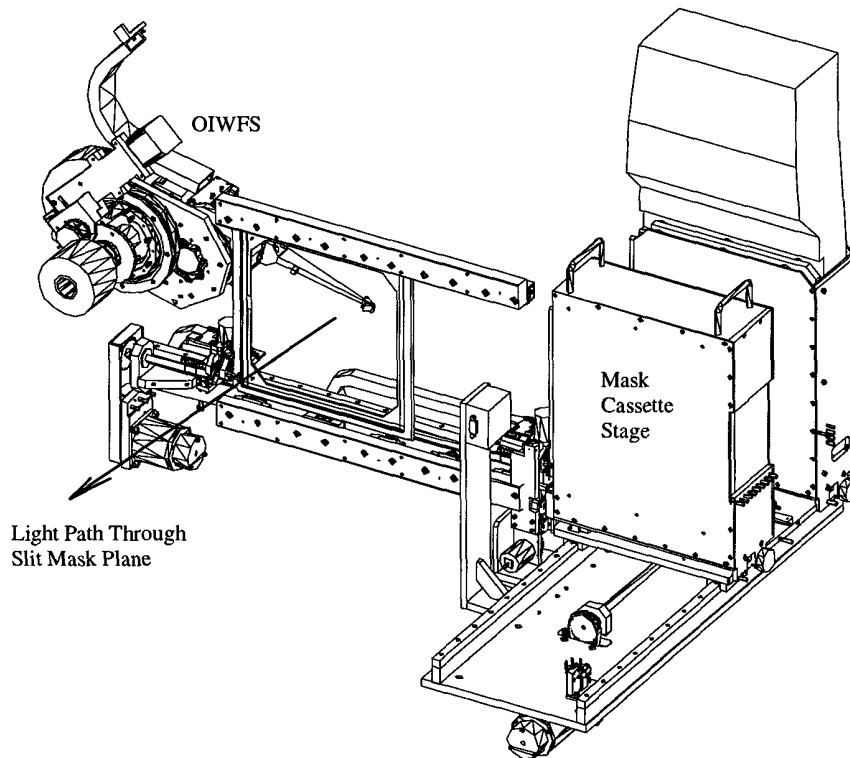


Figure 1 - GMOS slit plane showing OIWFS and mask handling system

The movement of the OIWFS guide probe is limited due to other mechanisms and structures in the GMOS slit plane environment. To avoid collisions, the motion of the guide probe must be limited to a sub-set of the kinematically possible motions of the stages. Therefore, a low resolution absolute position encoding scheme is required to determine the stage position at start-up to avoid probe damage. This encoding scheme operates outside of software control and will not permit the OIWFS to collide with other slit plane mechanisms.

2. OPTICAL DESIGN

The OIWFS feed optics produce a 3mm diameter image of the telescope exit pupil, located at the telescope secondary mirror, on the 2x2 Shack Hartmann lenslet array at the WFS. The delivered beam is collimated at the entrance to the lenslets. The optical design is shown in Figure 3. The incoming guide-star light at $f/16$ is intercepted by a fold prism with one powered face. It is then transmitted along the pickoff arm through a field stop to a doublet lens followed by an R band filter and finally into the WFS optics. In the figure, the location labelled 'edge' corresponds to the deepest point the pickoff arm will protrude into the GMOS CCD field. The pupil imaging lens had to be located to the right of this to avoid vignetting the field. The OIWFS stage mechanics were designed so that the feed optics stay pointed at the telescope exit pupil as the system patrols the field.

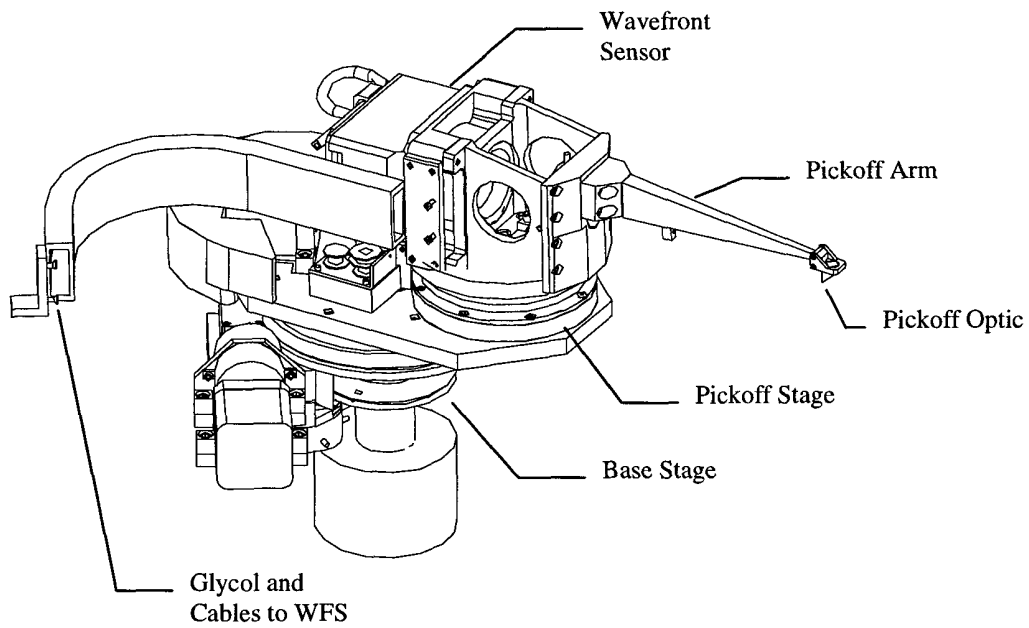


Figure 2 - GMOS On-Instrument Wavefront Sensor (OIWFS)

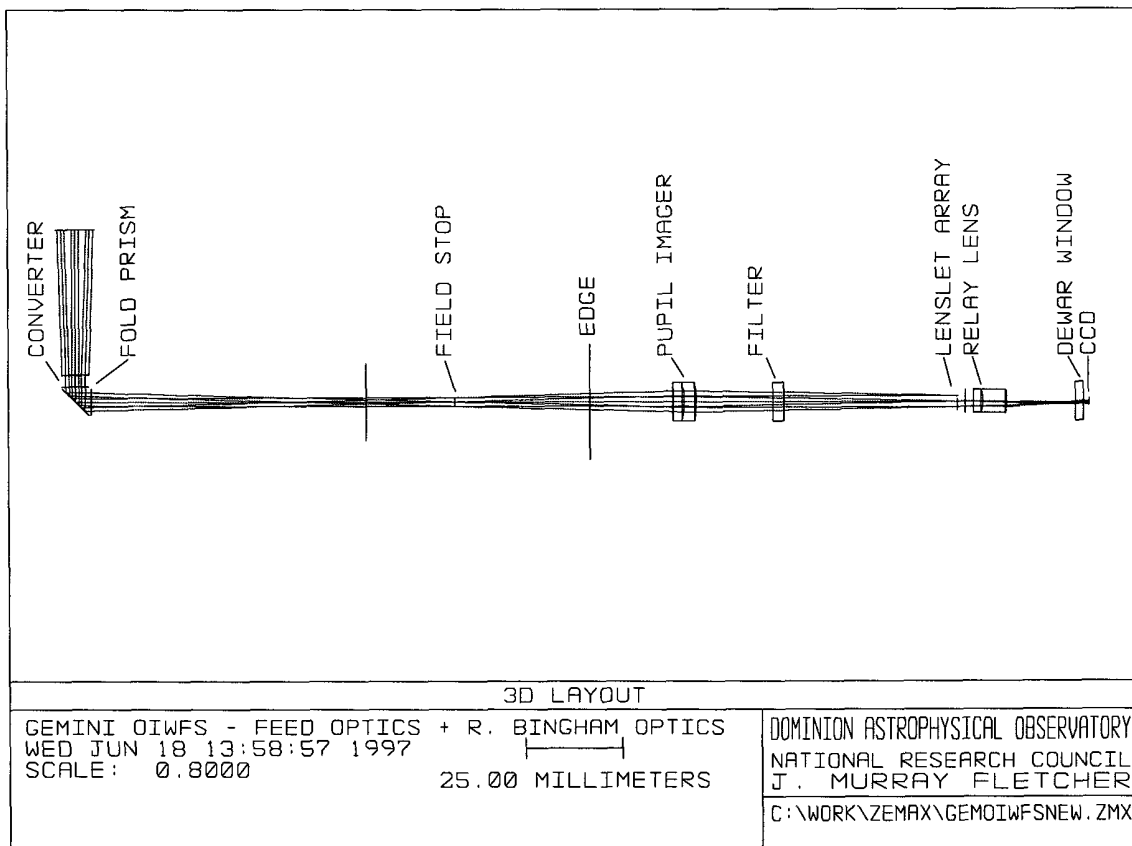


Figure 3 - OIWFS feed optical design with WFS optics

3. KINEMATICS

3.1 Stage Geometry

The OIWFS with associated coordinate systems is shown in Figure 4. Figure 5 shows the GMOS slit plane with the OIWFS patrol area. The full telescope beam passed to GMOS is 7 arcminutes in diameter. However, only the square 5.5 arcminute field is passed to the GMOS CCD detector. The OIWFS is capable of patrolling within the 7 arcminute field but outside the 5.5 arcminute field to allow non-vignetted guiding. Two OIWFS patrol areas are shown because the Cassegrain rotator can be turned 180° without varying the slit orientation. This allows the OIWFS to patrol a different region of the field. The 2 arcminute adaptive optics field is fully patrolled by the OIWFS. As the OIWFS patrols the GMOS field it is necessary keep the optical system pointed at the telescope exit pupil to avoid vignetting. This is accomplished by tilting the axes of the two rotational stages to point at the exit pupil. The notation used in this section follows the conventions used by Craig³.

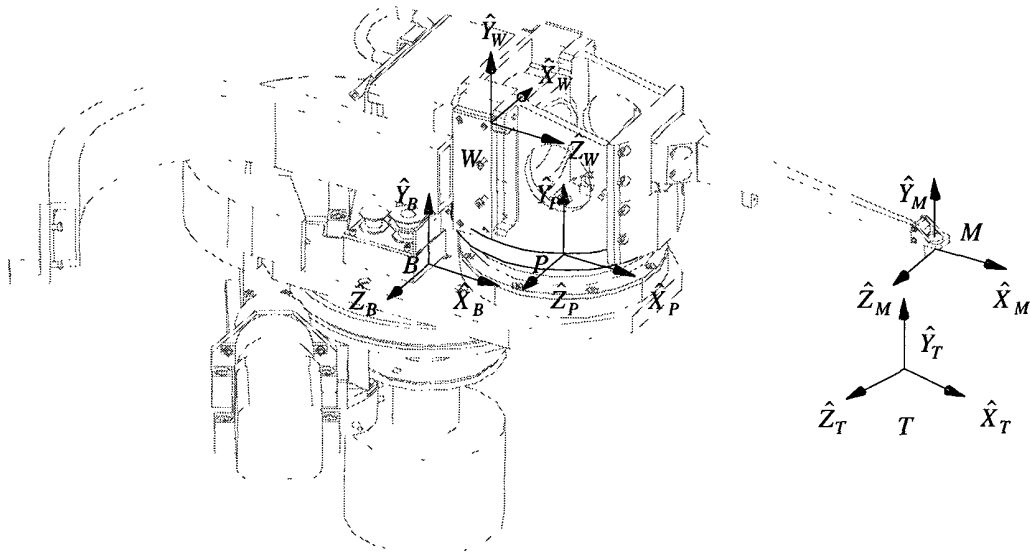


Figure 4 - OIWFS coordinate systems

Frame T , the telescope frame, is a fixed frame on the central axis of the telescope focal plane. Frame B , the base stage frame, is centred on the axis of the base stage bearing. The \hat{Y}_B axis defines the rotational axis of the base stage bearing and points at the centre of the telescope exit pupil. Frame P is centred on the rotational axis of the second stage bearing. The \hat{Y}_P axis also points at the telescope exit pupil. Frame M is located on the optical axis of the prism pickoff optic. The \hat{Y}_M axis points at the telescope exit pupil. Since the rotational axes of both stages point at the exit pupil, the \hat{Y}_M axis will stay pointed at the exit pupil as the OIWFS moves across the focal plane. Therefore the OIWFS will not vignette the exit pupil as it patrols the focal plane.

Rotations about the $\hat{X}, \hat{Y}, \hat{Z}$ axes are denoted α, β, γ respectively. All rotations are Euler angles, i.e., the rotations occur about the moving coordinate frame axes during a transformation. All linear distances are in millimetres.

The telescope exit pupil is positioned the distance D_p along the T frame Y axis where

$$D_p = 16400 \quad (1)$$

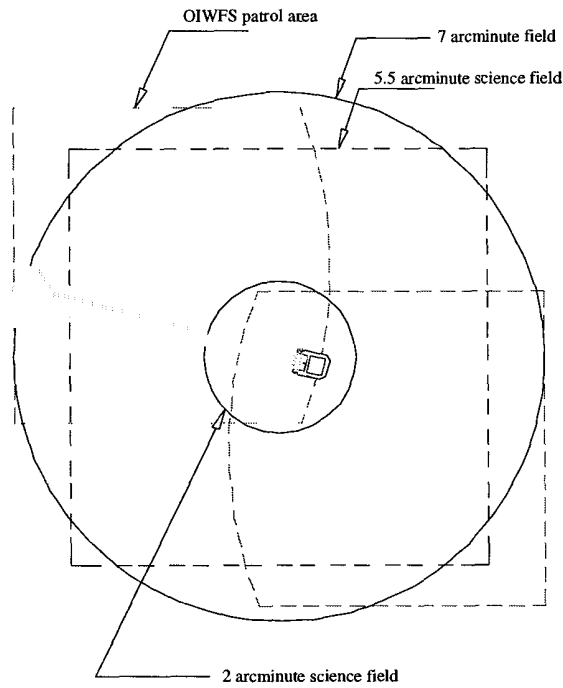


Figure 5 - OIWFS patrol area on the GMOS slit plane

The distance from T to B in T frame coordinates is

$$T_x = -265.30 \quad (2)$$

$$T_y = 17.58 \quad (3)$$

$$T_z = 63.20 \quad (4)$$

Given

$$T_{xz} = -\sqrt{T_x^2 + T_z^2} = -272.724 \quad (5)$$

The following relations define the rotational angles about frame B relative to frame T

$$\gamma_{tb} = \tan^{-1}(T_{xz} / D_p) = -0.953^\circ \quad (6)$$

$$\beta_{tb} = -\tan^{-1}(T_z / T_x) = 13.399^\circ \quad (7)$$

The rotation β_{tb} aligns the B frame so that the \hat{X}_B and \hat{Y}_B axes define a plane that passes through the origin of \hat{T} and the centre of the exit pupil. The rotation γ_{tb} points the \hat{Y}_B axis at the centre of the exit pupil. The transformation from T to B is accomplished by first translating by T_x, T_y, T_z and then rotating by β_{tb} , and then rotating by γ_{tb} . The resulting transformation, where C denotes cosine and S denotes sine, is

$${}^B_T = \begin{bmatrix} C(\beta_{tb}) \times C(\gamma_{tb}) & -C(\beta_{tb}) \times S(\gamma_{tb}) & S(\beta_{tb}) & Tx \\ S(\gamma_{tb}) & C(\gamma_{tb}) & 0 & Ty \\ -S(\beta_{tb}) \times C(\gamma_{tb}) & S(\beta_{tb}) \times S(\gamma_{tb}) & C(\beta_{tb}) & Tz \\ 0 & 0 & 0 & 1 \end{bmatrix} \quad (8)$$

The distances from B to P in B frame coordinates are

$$B_x = 77.50 \quad (9)$$

$$B_y = 29.62 \quad (10)$$

$$B_z = 0 \quad (11)$$

The rotation of frame P about the \hat{Z}_P axis to point \hat{Y}_P at the pupil centre is

$$\gamma_{bp} = \tan^{-1} \left[\frac{T_{xz} + B_x}{D_p} \right] - \gamma_{tb} = 0.271^\circ \quad (12)$$

The transformation from a point in the base frame to the pickoff bearing frame is given in equation 13. The transformation is accomplished with a rotation of β_{bp} , the stage rotation angle, followed by a translation of B_x , B_y , B_z followed by a rotation of γ_{bp} .

$${}^P_T = \begin{bmatrix} C(\gamma_{bp}) \times C(\beta_{bp}) & -S(\gamma_{bp}) \times C(\beta_{bp}) & S(\beta_{bp}) & C(\beta_{bp}) \times B_x \\ S(\gamma_{bp}) & C(\gamma_{bp}) & 0 & B_y \\ -C(\gamma_{bp}) \times S(\beta_{bp}) & S(\gamma_{bp}) \times S(\beta_{bp}) & C(\beta_{bp}) & -S(\beta_{bp}) \times B_x \\ 0 & 0 & 0 & 1 \end{bmatrix} \quad (13)$$

The distances from P to M in P frame coordinates are

$$P_x = 213.03 \quad (14)$$

$$P_y = 64.03 \quad (15)$$

$$P_z = 0 \quad (16)$$

The rotation of frame M about the \hat{Z}_M axis to point \hat{Y}_M at the pupil centre is

$$\gamma_{pm} = \tan^{-1} \left[\frac{T_{xz} + B_x + P_x}{D_p} \right] - \gamma_{tb} - \gamma_{bp} = 0.744^\circ \quad (17)$$

The transformation from a point in the pickoff frame to the mirror frame is accomplished by a rotation β_{pm} , the stage rotation angle, followed by the rotation γ_{pm} , followed by a translation of P_x , P_y , P_z and is given in equation 18.

$${}^M_P T = \begin{bmatrix} C(\gamma_{pm}) \times C(\beta_{pm}) & -S(\gamma_{pm}) \times C(\beta_{pm}) & S(\beta_{pm}) & C(\gamma_{pm}) \times C(\beta_{pm}) \times Px - S(\gamma_{pm}) \times C(\beta_{pm}) \times Py \\ S(\gamma_{pm}) & C(\gamma_{pm}) & 0 & S(\gamma_{pm}) \times Px + C(\gamma_{pm}) \times Py \\ -C(\gamma_{pm}) \times S(\beta_{pm}) & S(\gamma_{pm}) \times S(\beta_{pm}) & C(\beta_{pm}) & -C(\gamma_{pm}) \times S(\beta_{pm}) \times Px + S(\gamma_{pm}) \times S(\beta_{pm}) \times Py \\ 0 & 0 & 0 & 1 \end{bmatrix} \quad (18)$$

The mapping from a point in the telescope frame to a point in the mirror frame is therefore

$${}^M P = {}^M_P T \times {}^P_B T \times {}^B_T T \times {}^T P \quad (19)$$

and the mapping from a point in the mirror frame to a point in the telescope frame is

$${}^T P = {}^B_T T^{-1} \times {}^P_B T^{-1} \times {}^M_P T^{-1} \times {}^M P \quad (20)$$

The invariance of the pupil pointing can be verified by transforming the coordinate of the exit pupil in T frame coordinates to the M frame using equation 19 and observing that \hat{X}_M and \hat{Y}_M remain zero as the stage angles β_{bp} and β_{pm} are varied to position the pickoff arm at various points in the telescope field.

3.2 Inverse Kinematics

The OIWFS inverse kinematics calculate the stage angles (β_{bp}, β_{pm}) required to position the pickoff at a point in the telescope field $({}^T P_x, {}^T P_y)$. Except for the outer radius of the pickoff field there are two sets of joint angle solutions for each telescope field location. However, further constraints, such as the bend angle of the cables and glycol lines to the WFS and the current position of the OIWFS will make one of the solutions more desirable. The control system for the OIWFS must evaluate the bend angle of the umbilical and the time required to move from the current to the new position and decide how the move will proceed. In one mode of operation, called non-sidereal tracking, the OIWFS must track a guide object that is moving relative to the object of interest. An example of this would be taking spectra of a comet, using a nearby star for guiding. The OIWFS would move throughout the exposure so as to keep the image comet stationary on the GMOS slit plane. In this case the stage angles for the whole exposure would be considered to determine the best choice. The inverse kinematics presented in this section do not consider the tilt angles of the stages. This results in a maximum error of 2 arcseconds within the patrol area of the OIWFS.

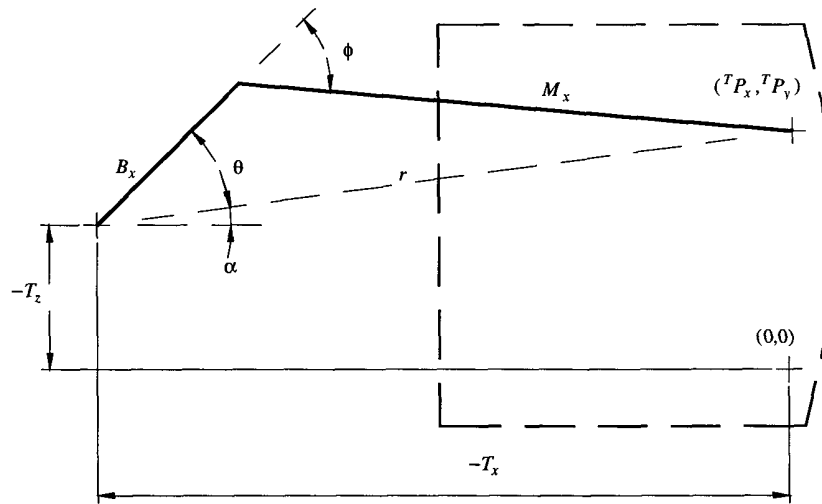


Figure 6 - OIWFS stage geometry for simplified inverse kinematics

The radius r , from the base stage is given in equation 23. Note that if $r > B_x + M_x$ or $r < M_x - B_x$ there is no solution.

$$X' = -T_x + T P_x \quad (21)$$

$$Y' = T_z + T P_y \quad (22)$$

$$r = \sqrt{X' + Y'} \quad (23)$$

The relevant angles are calculated as follows

$$\alpha = a \tan 2(X', Y') \quad (24)$$

$$\phi = \cos^{-1} \left[\frac{r^2 - (B_x^2 + M_x^2)}{2B_x M_x} \right] \quad (25)$$

$$\theta = \begin{cases} \left(\pi - \sin^{-1} \left[\frac{M_x \sin \phi}{r} \right] \right); \text{if } (M_x^2 > r^2 + B_x^2) \\ \sin^{-1} \left[\frac{M_x \sin \phi}{r} \right]; \text{otherwise} \end{cases} \quad (26)$$

The two solutions are

$$\begin{cases} \beta_{bp} \\ \beta_{pm} \end{cases} = \begin{cases} -\theta - \alpha + \beta_{tb} \\ \phi \end{cases} \quad (27)$$

$$\begin{cases} \beta_{bp} \\ \beta_{pm} \end{cases} = \begin{cases} \theta - \alpha + \beta_{tb} \\ -\phi \end{cases} \quad (28)$$

4. FLEXURE ANALYSIS

4.1 Pickoff Arm Flexure Analysis

The GMOS pickoff arm is designed to rigidly position a small pickoff optic in front of the slit plane while minimizing the vignetting of the science field. In order to predict the performance of the OIWFS, the arm and optic cell flexure must be fully understood. As described below, a model was used to calculate the flexure of the pickoff arm as a function of instrument orientation or gravity vector. The model was verified against analytical and finite element analysis (FEA) solutions.

The GMOS pickoff mechanics consist of a rigid arm with an optical mounting cell attached to the end. The arm, a double tapered beam, maintains a rectangular cross-section but the width and height decrease linearly along the length towards the mirror mount. The beam is also tapered in the direction of the optical axis slightly more than the $f/16$ focal ratio to avoid reflections off the side of the arm. A MathCAD worksheet was created to model the deflections and rotations of the pickoff mirror as a function of gravity vector. The deflection and slope at the end of the beam are calculated by integrating the general differential equation (29) for beam bending relating the elastic modulus E , moment of inertia of area I , and moment M to the second derivative of displacement along the beam.

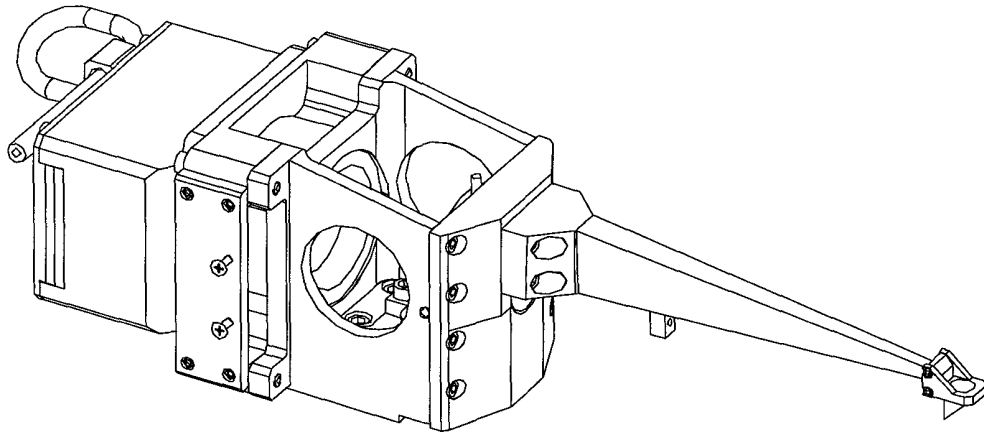


Figure 7 - OIWFS pickoff arm and WFS assembly

This calculation was performed twice, once for the beam self weight, and once for the point load at the end of the beam. The two solutions were added to obtain the overall deflection and slope. A complication that led to a numerical computation of flexure and slope was the fact that I is a function of the varying beam cross-section. For the self-weighted case, M also varies as a function of beam geometry.

$$EI \frac{d^2y}{dx^2} = M \quad (29)$$

The numerical model considers beam self-loading and a point load at the end of the beam to represent the pickoff mirror assembly. The numerical solution was checked against several analytical solutions for invariant cross-section and singly tapered beams and the results agreed to within a few percent. The model calculated beam deflection and slope about two orthogonal axes and, since the pickoff optic centre of gravity is off the central beam axis, torsion along the length of the beam. The effect of the beam deflections and rotations are evaluated at the pickoff mirror. The focal plane vignetting for the fully extended pickoff arm was also calculated. The GMOS functional requirements allowed a maximum vignetting of 5% of the focal plane.

Sensitivity factors that relate pickoff mirror deflections and rotations to WFS measurement errors were derived. These sensitivities were checked using RayCAD raytracing software within AutoCAD. WFS measurement errors can be expressed as errors on the sky in milli-arcseconds (MAS). The model calculates the absolute error for the range of possible gravity vectors to 60° off zenith in 15 degree increments in altitude and azimuth. From this data the maximum error on the sky per 15 degrees of telescope tracking can be calculated.

The model was used to calculate gravity-induced WFS measurement errors for a number of beam geometries that vignette the focal plane equally (4.5%). This permitted optimization of the beam design to minimize OIWFS measurement errors due to pickoff flexure. Further restrictions on the beam geometry were that it could not be less than 4mm in width or height at the pickoff mirror end and that it could not be more than 22.5 mm in height at the mount end. These conditions were based on packaging and manufacturing requirements.

The linear deflections of the pickoff arm optic are denoted X_{PM}, Y_{PM}, Z_{PM} and the rotational deflections are denoted $\alpha_{PM}, \beta_{PM}, \gamma_{PM}$. The optical length from the pickoff optic to the entrance to the WFS is denoted L (240 mm). The errors introduced in the WFS measurement by the flexure of the pickoff arm are

$$E_p = \begin{bmatrix} 0 & 0 & 0 \\ -1 & 1 & 0 \\ 1 & -1 & 0 \end{bmatrix} \begin{bmatrix} X_{PM} \\ Y_{PM} \\ Z_{PM} \end{bmatrix} + \begin{bmatrix} -L & -L & 0 \\ 0 & 0 & -2L \\ 0 & 0 & 0 \end{bmatrix} \begin{bmatrix} \alpha_{PM} \\ \beta_{PM} \\ \gamma_{PM} \end{bmatrix} \quad (30)$$

Several materials were evaluated for the pickoff arm

Material	CTE ($C \times 10^{-6}$)	Young's Modulus (E)	Poisson's Ratio (ν)	Shear Modulus (G)	Density (ρ) (gm/cm^3)	Specific Stiffness (E/ρ)	Pickoff Relative Performance
Beryllium	11.3	290.0	0.027	141.2	1.9	156.8	1.000
Molybdenum	5.0	320.0	0.320	121.2	10.2	31.3	2.344
Steel (1015)	11.9	193.0	0.287	75.0	7.8	24.9	2.971
Titanium	8.8	114.0	0.340	42.5	4.4	25.7	3.727
Aluminum (7075)	23.4	71.7	0.332	26.9	2.8	25.7	4.637
Magnesium	25.2	44.8	0.350	16.6	1.8	25.3	6.200
Invar 36	0.3	147.0	0.290	57.0	8.1	18.1	4.314

Table 1 - Pickoff arm material evaluation

Although beryllium was by far the best performing material, steel met the design requirements and was chosen for cost and ease of manufacturing. Note that because the pickoff mirror is subject to an end load as well as self-loading, the pickoff performance does not scale directly with specific stiffness. In fact, more dense materials with the same specific stiffness perform better than less dense ones.

The OIWFS errors attributable to pickoff arm flexure are shown in Figure 8. The vertical axis of the plot is error in MAS. The horizontal axes are angle steps of 15 degrees in an altitude-azimuth coordinate system that covers telescope observations to 60 degrees off zenith. The maximum OIWFS error due to the pickoff arm flexure is 1.3 milli-arcseconds per hour of telescope tracking.

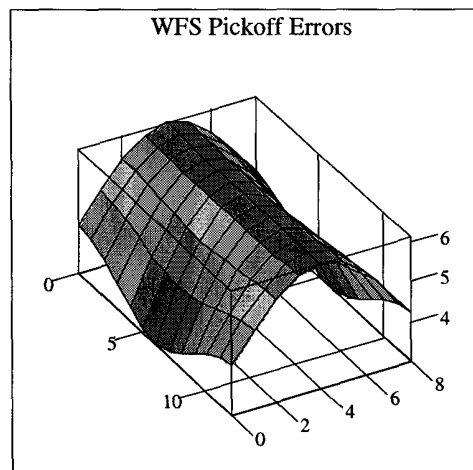


Figure 8 - pickoff arm error contribution

4.2 Bearing Flexure Analysis

As shown in Figure 4, the OIWFS is positioned on the slit plane using two stacked rotary stages. Rotational stages have attractive properties for design of high precision mechanisms that have low sensitivity to gravity vector changes. If a rotational stage is balanced so that the centre of gravity of the carried mass falls on the central axis of bearing rotation, there will be no tendency for the stage to rotate as the gravity vector changes. This is impossible to accomplish with a linear stage without relatively complex counterbalance systems. In addition, by using a preloaded bearing and further balancing masses to minimize certain modes of bearing flexure, the rotational stage can be designed to flex minimally with gravitational load. The OIWFS stage was designed with these principles in mind. Both rotational stages are mass balanced to reduce or eliminate moment type bearing loads in favour of straight radial and axial loads. The stage bearings are dominant in error contribution to the OIWFS stage performance. It is believed that the stage mechanics, other than the pickoff arm and bearings, can be designed with essentially no flexure or error contribution to the OIWFS error budget. Therefore, this section deals solely with the OIWFS stage bearing flexure.

Bearing selection requirements included high stiffness and compact design. The most suitable bearing for the application was found to be the Kaydon Type X four point contact bearings. In the Type X bearing, each roller contacts at four points, two on the outer and two on the inner race. The contact pattern allows a single bearing to be stiff in radial, axial and moment modes. Also, preloaded assemblies are available with the balls slightly oversized so that there is an interference fit between the inner and outer races. A single preloaded Type X bearing was chosen for each of the two OIWFS stages.

A MathCAD spreadsheet was developed to calculate the linear and rotational motion of the pickoff optic due to bearing flexure. As with the analysis of the pickoff arm, the WFS sensitivities to these motions were calculated. In this case, the pickoff optic and WFS move as a solid body. The linear deflections of the pickoff arm optic due to bearing flexure are denoted X_{BM}, Y_{BM}, Z_{BM} and the rotational deflections are denoted $\alpha_{BM}, \beta_{BM}, \gamma_{BM}$.

$$E_B = \begin{bmatrix} 0 & 0 & 1 \\ -1 & 0 & 0 \\ 0 & -1 & 0 \end{bmatrix} \begin{bmatrix} X_{BM} \\ Y_{BM} \\ Z_{BM} \end{bmatrix} + \begin{bmatrix} -L & 0 & 0 \\ 0 & 0 & -L \\ 0 & 0 & 0 \end{bmatrix} \begin{bmatrix} \alpha_{BM} \\ \beta_{BM} \\ \gamma_{BM} \end{bmatrix} \quad (31)$$

The OIWFS errors attributable to bearing flexure are shown in Figure 9. The vertical axis of the plot is error in milli-arcseconds. The maximum OIWFS error due to bearing flexure is 0.4 milli-arcseconds per hour of telescope tracking.

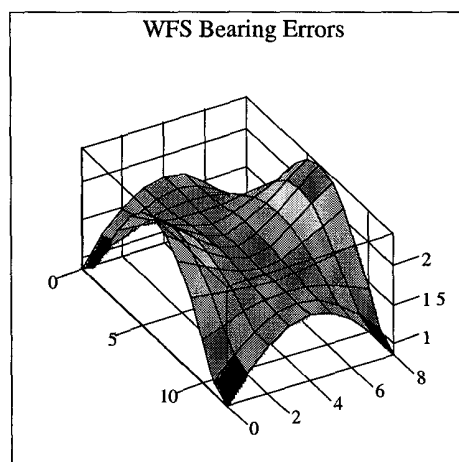


Figure 9 - OIWFS bearing error contribution

4.3 Overall Performance

The absolute measurement error of the OIWFS is calculated in milli-arcseconds on the sky by the following relation where S

$$E_S = \begin{bmatrix} 1/S & 0 & 0 \\ 0 & 1/S & 0 \\ 0 & 0 & 1/SF \end{bmatrix} \left[E_P + E_B \right] \quad (32)$$

is the image scale at the slit plane ($621\mu\text{m} / \text{arcsec}$) and F is the focal ratio of the telescope ($f/16$).

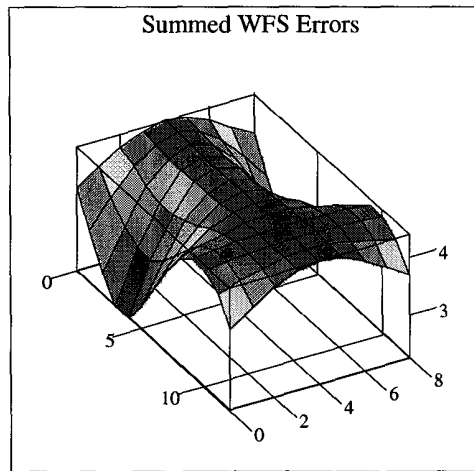


Figure 10 - Total OIWFS error contribution

The combined errors introduced into the OIWFS by the pickoff arm and WFS bearings are shown in Figure 10. The vertical axis of the plot is error in milli-arcseconds. The overall error per hour of telescope tracking time is less than the error due to the pickoff arm alone. This is due to the way the bearing and pickoff arm errors add, resulting in a lower slope over the surface of the error map. The total contribution of error to the OIWFS measurement from pickoff arm and bearing flexure is calculated to be 0.9 milli-arcseconds per hour of telescope tracking. This equates to $0.6 \mu\text{m} / \text{hr}$ error at the GMOS slit plane, well within the specification of $2.05 \mu\text{m} / \text{hr}$.

5. ACKNOWLEDGEMENTS

We thank to our colleagues at DAO, ROE, RGO and the University of Durham, and the Gemini Project Office.

6. REFERENCES

- ¹ R. Davies, J.R. Allington-Smith, et. al., "GMOS: The Gemini Multiple Object Spectrographs", *Optical Telescopes of Today and Tomorrow*, A. Ardeberg, ed., SPIE Volume 2871, pp. 1284-1294, 1996.
- ² J.R. Allington-Smith, R. Content, R. Haynes, I.J. Lewis, "Integral field spectroscopy with the Gemini Multiobject Spectrographs", *Optical Telescopes of Today and Tomorrow*, A. Ardeberg, ed., SPIE Volume 2871, pp. 1099-1106, 1996.
- ³ J. Craig, *Introduction to Robotics, Mechanics and Control, 2nd Edition*, pp. 16-17, Addison Wesley, 1989.